Lasso Peptides: Exploring the Folding Landscape of Nature's Smallest Interlocked Motifs

Gabriel C. A. da Hora,[1] Myongin Oh,[1†] Marcus C. Mifflin,[1] Lori Digal,[1§] Andrew G. Roberts,[1] and Jessica M.J. Swanson[1]*

[1]Department of Chemistry, University of Utah, Salt Lake City, UT, 84112 – United States of America

ABSTRACT

Lasso peptides are a class of natural products characterized by a threaded structure. Given their small size and stability, chemical synthesis would offer tremendous potential for the development of novel therapeutics. However, the accessibility of the pre-folded lasso architecture has limited this advance. To better understand the folding process *de novo*, simulations are used herein to characterize the folding propensity of microcin J25 (MccJ25), a lasso peptide known for its antimicrobial properties. New algorithms are developed to unambiguously distinguish threaded from non-threaded precursors and determine handedness, a key feature in natural lasso peptides. We find that MccJ25 indeed forms right-handed pre-lassos, in contrast to past predictions but consistent with all natural lasso peptides.

Additionally, the native pre-lasso structure is shown to be metastable prior to ring formation but to readily transition to entropically-favored unfolded and non-threaded structures, suggesting *de novo* lasso folding is rare. However, by modifying the ring forming residues with the appendage of thiol and thioester functionalities, we are able to increase the stability of pre-lasso conformations. Furthermore, conditions leading to protonation of a histidine imidazole side chain further stabilize the modified pre-lasso ensemble. This work highlights the use of computational methods to characterize lasso folding and demonstrates that *de novo* access to lasso structures can be facilitated by optimizing sequence, unnatural modifications, and reaction conditions like pH.

INTRODUCTION

Lasso peptides are an expanding class of compact bioactive ribosomally synthesized and post-translationally modified peptide natural products (RiPPs) characterized by an interlocked lasso fold.[1-4] These cyclic entangled structures (**Figure 1**) can range from 13-33 residues in length[5, 6] and result from an isopeptide bond between the *N*-terminal amine and a side chain carboxylate, which forms a 7-9 residue macrolactam ring that is threaded by the *C*-terminal peptide tail.[2, 5-7] Once folded and cyclized, lasso peptides are extremely stable with their threaded tails held below the ring by steric locks, called plugs, formed by bulky side chains.[8] In biological systems, lasso peptide maturation begins with the lasso precursor leader sequence

to a RiPP precursor recognition element (RRE) that guides its cleavage by a leader peptidase, which enables a lasso cyclase to fold the lasso motif and catalyze the isopeptide bond formation.[1, 3, 9, 10] Once formed, the value of lasso peptides in nature is demonstrated by their diverse biological activities, including enzyme inhibition, receptor antagonism, and antibiotic effects,[4, 11-14] which are likely facilitated by their thermal stability, resistance to degradation, and rigid globular shapes.[4, 15, 16] Accordingly, the lasso scaffold could be invaluable in the design of novel therapeutics that are sized between small molecules and biologics,[15, 17] which can lead to reduced immunogenicity and the capacity for bioavailibility.[3, 13, 18-20] Collectively, lasso peptides warrant further investigation.

The production of lasso peptides has been considerably expanded through the development of heterologous expression and cell-free biosynthesis approaches.[3, 7, 16, 21, 22] However, an adaptable chemical synthesis platform would provide further access to this scaffold and unnatural variants.[23, 24] A central limitation in the development of a chemical synthesis platform is the requirement that the lasso precursor be pre-folded prior to isopeptide bond formation; otherwise, the non-threaded conformation (herein referred to as a tadpole) would be obtained.[15, 18] Indeed previous direct cyclization attempts to access lasso peptides have exclusively given the non-threaded tadpole isomers.[15, 25-29] While biological systems stabilize the pre-lasso fold through an enzyme-substrate complex, the outstanding question explored in this work is whether the lasso precursor can also be sufficiently stabilized through the intramolecular forces that dictate peptide and protein folding.

Previous work on microcin (MccJ25), a bacterial RNA polymerase inhibitor[12, 26, 30-35] suggested it forms an unnatural left-handed pre-lasso peptide (**Figure 1**).[25] This was unexpected given that MccJ25 and every other structurally characterized lasso peptide is right-handed in nature (**Figure 1**).[25, 36] Herein we revisit the folding propensity of MccJ25 using modern simulation approaches to enable the development of generalized tools for studying pre-lasso folding and supporting future lasso peptide chemical synthesis efforts.

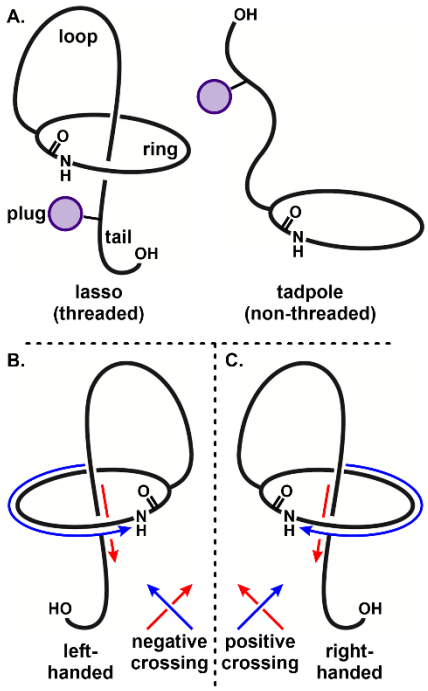

Figure 1: **A.** Possible conformations for the peptide after the formation of the isopeptide bond: lasso (threaded tail) or tadpole (non-threaded tail). Prior to bond formation, the pre-lasso conformation can have **B.** left-handed (counterclockwise) or **C.** right-handed configurations (clockwise). The blue colored arrows indicate the directionality of the *N*-

terminus-based ring closure, counterclockwise and clockwise, with respect to the threaded tail directionality (red arrows) kept constant.

We find that native MccJ25 forms the anticipated natural right-handed pre-lasso conformation, and verify that the previous findings[25] were a consequence parameter issues in the GROMOS96 43A2 forcefield.[37-40] We present new tools that unambiguously distinguish pre-lasso from non-lasso structures and differentiate the right- and left-handed forms.[41] We further describe several collective variables that discretize the pre-lasso folding landscape for distinguishing the threaded pre-lasso from the non-threaded pre-tadpole conformations. We find that the barrier for escape from the pre-lasso conformation is only ~1.5 kcal/mol while the probability for reaching the pre-lasso state is less than 1% for the native sequence. Thus, the probability of *de novo* folding is extremely low. However, with the addition of chemical modifications to the isopeptide bond-forming residues, we stabilize the pre-lasso fold. Additionally, upon protonation of a histidine residue in the ring, we further stabilize the pre-lasso state, which indicates that reaction conditions such as pH can influence the folding landscape. Collectively, this work demonstrates how *de novo* lasso peptide folding can be facilitated by sequence deviations, chemical modifications, and reaction conditions, which can provide novel opportunities to guide future synthetic approaches.

RESULTS AND DISCUSSION

Lasso Threading Classification and Handedness Descriptor

To characterize a lasso folding landscape we first had to develop methods that clearly distinguish regions of phase space that form the threaded isomer (pre-lasso structures) from regions that form the non-threaded variant (pre-tadpole conformations). As discussed below, this has been particularly challenging in past analyses. To address this challenge, we first defined structures capable of forming an isopeptide bond (pre-ring structures) as those with a separation of 6 Å or less between Gly1N and Glu8Cδ. All structures with separations larger than 6 Å were designated as unfolded. We next needed an approach capable of identifying structures in which the tail pierces through the pre-ring. Inspired by the minimal surface analysis used to locate complex lasso proteins from the Protein Data Bank (PDB),[41, 42] we developed a triangulation-based algorithm to evaluate the position of the tail with respect to the pre-ring (**Supporting Information - Methods**). This analysis divides the pre-ring (residues 1 to 8 of MccJ25) into a series of triangles (**Figure 2**) that are then evaluated for points of intersection by the line segments connecting consecutive residues in the loop/tail (residues 14 to 20) using barycentric coordinates. Although it is not a differentiable variable, this algorithm unambiguously delineates pre-lasso from pre-tadpole conformations.

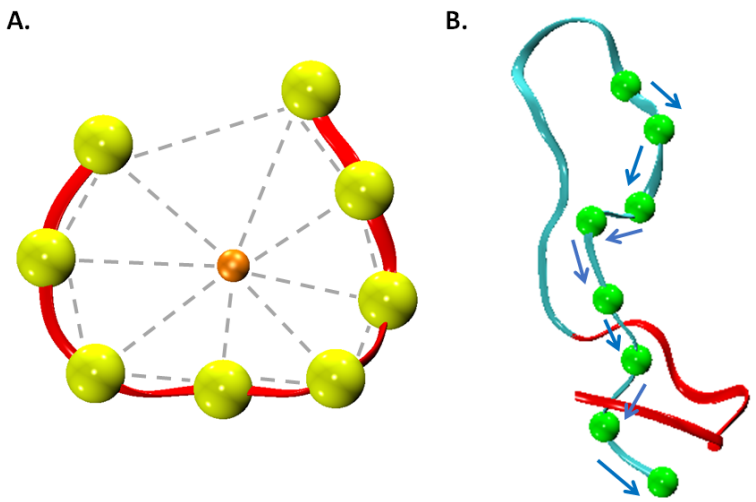

Figure 2: Lasso threading classification: **A.** Triangulation of the ring area formed by residues 1 to 8 of MccJ25. The ring and the triangles are shown with red and dotted gray lines, respectively. The alpha carbon atoms and the center of mass of the ring are represented by yellow and orange spheres, respectively. **B.** Discretization of the piercing tail formed by residues 14 to 20 of MccJ25. The peptide is represented by a cyan ribbon, but the ring is red for clarity. The alpha carbon atoms are represented by green spheres, and each line segment is shown as a blue arrow.

We next had to develop a tool that could definitively distinguish left- from right-handed pre-lasso conformations (**Figure 1**). We developed a handedness descriptor, κ, that leverages the orientation of the ring encirclement relative to the directionality of the tail: if the N-terminus wraps around the tail in a clockwise manner, it is right-handed and vice versa. By projecting the vectors connecting ring alpha carbons onto the plane normal to the tail (**Figure 3**) and evaluating their cross products with the vector connecting tail piercing alpha carbons

20 to 19 using a summation of dot products, which makes κ positive for right-handed conformations and negative for left. Both tools, the lasso threading classification algorithm and handedness descriptor, are fully described in **Methods** and available at https://github.com/gabedahora/LATCHED (Lasso Threading Classification and Handedness Evaluation Descriptor).

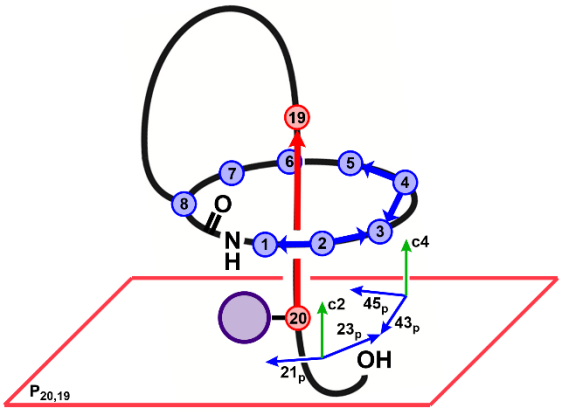

Figure 3: Lasso handedness descriptor for right-handed conformation of MccJ25. The black line shows the backbone of the lasso peptide. The red square is the plane with its normal vector (red arrow) connecting residues 20 and 19 (red dots). The relevant vectors (blue arrows) for residues 2 and 4 (ring alpha carbons in blue dots) and their projections on the plane are shown (*e.g.*, $\mathbf{21_P}$). The green arrow shows the cross-product of the two projected vectors.

Folding of MccJ25

As the most stringent test, we first performed unbiased MD simulations starting from an extended linear conformation to assess the ability of MccJ25 to fold with minimal bias on the

preferred structures. No pre-lasso structures were observed in 7.2 μs, but pre-tadpoles and pre-macrocycles (defined by distances of 6 Å or less between Gly1-Gly21) were detected, representing ~3% (21,288 structures) of the sampled phase space. The *DBSCAN* cluster analysis[43] identified four structural clusters (**Figure S1**). Two clusters, 1 and 2, contained pre-macrocycles without the characteristic β-hairpin secondary structure that is unique to MccJ25,[15, 25] including some with a short alpha-helix (cluster 2). The other two clusters, 0 and 3, contained pre-tadpole structures with the β-hairpin secondary structure, indicating the formation of this structure is readily accessible in unbiased simulations when starting from an extended conformation. This antiparallel beta structure is formed by hydrogen bonds between residues 7-16. Thus, while lasso folding and cyclization are enzyme-stabilized in nature,[7, 15, 18] the β-hairpin formation is accessible in the absence of enzymes, suggesting a potential pathway for *de novo* pre-lasso folding.

We next investigated the unfolding process starting from the native MccJ25 structure (PDB ID 1Q71)[26] with the covalent isopeptide bond between residues Gly1 and Glu8 hydrolyzed to examine how readily it transitions to pre-tadpole and unfolded structures (**Figure 4**). For eight replicas, the pre-lasso configuration remained stable for ~150-500 ns, which is notably longer than the previously reported unfolding in less than 4 ns.[25] Within this shallow metastable basin, the distance between residues Gly1 and Glu8 fluctuates apart and returns to the pre-lasso state while the β-hairpin remains stable. During this time, approximately half of the replicas included the formation of transient pre-tadpoles but returned to pre-lassos. After ~500 ns, the β-hairpin is lost, and the system does not return to a pre-lasso form in 7.2 μs (**Figure 4**),

which is also demonstrated in the secondary structure map (**Figure S2**). Thus, a metastable minimum containing pre-lasso structures does exist, but it represents less than 1% of the above sampled conformations (**Table S1**), suggesting it is rare relative to the entropically-favored unfolded phase space.

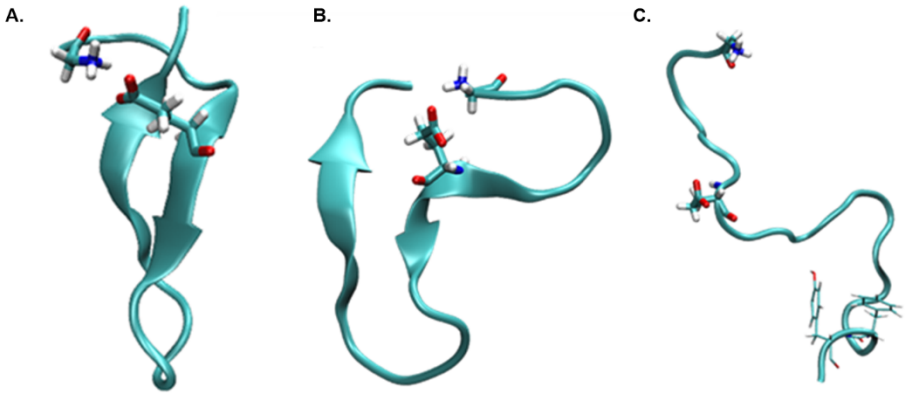

Figure 4: Representative configurations of MccJ25 in unbiased simulations: **(A)** starting pre-lasso (t = 0 ns); **(B)** fluctuating between pre-lasso and pre-tadpole (t < 500 ns); **(C)** completely unfolded (t > 500 ns).

Assessing MccJ25 Handedness

In their 2010 study,[25] Ferguson *et al.* applied a powerful nonlinear dimensionality reduction approach called diffusion map[44] to characterize the conformations obtained in 90 ns of replica exchange MD (REMD) combined with short 30 ns unbiased simulations starting from conformations approaching left- and right-handed pre-lassos. Similar to Yang *et al.,*[45] they

defined a physical order parameter Λ for the MccJ25 β-hairpin as the average length of the seven vectors connecting alpha carbons of adjacent residues 6-20 λ_i=1…7: (λ_1 for Val6-Tyr20, λ_2 for Pro7-Phe19, etc. - **Figure 5**):

$$\Lambda = \frac{1}{7} \sum_{i=1\cdots7} \lambda_i \qquad (3)$$

Figure 5: Representation of parameter Λ quantifying the formation of the β-hairpin as the average length of the seven vectors connecting alpha carbons of the loop residues 6 to 20.

Consequently, an increase in Λ corresponds to a lengthening of the λ_i distances and decreased hydrogen bonding in the β-hairpin. The other parameter used to define phase space was the Glu8 Ψ angle, which was estimated to be around -80° for right-handed structures and 90° for left ones. Using the same parameters, we evaluated our simulations and found similar dominant Ψ angles of -24°/-33° and 155°/145° for structures with/without the isopeptide bond intact, suggesting even after the bond is broken the pre-lasso retains right-handed structures (**Figure S3**). However, it was not clear if the Glu8 Ψ angle could delineate handedness. This

motivated our development of the lasso handedness descriptor, κ, which definitively distinguishes right- and left-handed structures **(Figure 3)**. This descriptor confirmed that no left-handed configurations were obtained in any of our ten replicas. In the previous work, left-handed structures remained stable for 30 ns with $\Lambda = 6.2 \pm 0.3$ Å and Glu8 $\Psi = 90 \pm 20°$. Filtering our ensembles through Λ values, we found a considerable diversity of pre-tadpoles and unfolded structures, but no left-handed pre-lassos.

To ensure we had comparative sampling, despite much longer unbiased simulations, we additionally performed temperature REMD with comparable parameters to those previously used. We were able to obtain 0.82% pre-lasso structures at 300K. Including the filtered structures (those with Gly1 Glu8 distances less than 6 Å) from higher temperatures, the percentage of pre-lassos decreases to 0.08% (**Table S1**), supporting the notion that entropy disfavors the pre-lasso fold. However, all the obtained pre-lassos were right-handed, consistent with those observed in nature. Collectively, these results suggest that the right-handed MccJ25 pre-lasso conformation is a metastable state that is accessible from the unfolded landscape, while the left-handed MccJ25 pre-lasso conformation is inaccessible. Additionally, the pre-tadpole structures significantly outnumber the pre-lasso structures, consistent with experimental observations of only tadpole structures from de novo folding.[25, 28]

These contrasting results to those previously reported[25] led to an investigation of the potential influence of the force fields used. The same system and simulation parameters were implemented with three other modern protein force fields: AMBER ff14SB,[46] CHARMM36,[47] and CHARMM36m.[48] The number of filtered structures where Gly1N to Glu8Cδ is ≤ 6 Å was

similar among the different force fields, all with right-handed pre-lasso structures. Relatively more pre-tadpole and unfolded structures were obtained in the simulations with both CHARMM force fields, but this was expected with CHARMM36m since it is optimal for intrinsically disordered proteins (**Table S1**). We also compared contact maps of the first eight residues (**Figure S4**) and found a similar interaction pattern among the tested force fields, with a slight increase in the side chain interactions for the AMBER force fields. Thus, the results between each of the modern force fields tested were consistent. Next, we used the GROMACS 2019.4[49] simulation engine to repeat the previously reported simulations with the same force field.[25] In these simulations, the right-handed pre-lasso rapidly transitions to unfolded (11 ns) and later to left-handed pre-lasso structures (3.0 μs). These results verify that the force field used in the previous study was the cause of the unexpected findings. GROMOS 43A2[50] was a state-of-the-art force field in 2010 but has since been updated and reparametrized to address numerous issues,[37-40] especially new Φ/Ψ torsional angle terms.[38] Thus, previous predictions of left-handed folding were due to force field artifacts. MccJ25 folds into the native right-handed pre-lasso structure with modern force fields, suggesting *de novo* lasso folding can be accessed without the aid of an enzyme, albeit rarely.

Discretization of the lasso folding landscape

Characterizing the lasso folding landscape requires both extensive sampling and discretization into regions that distinguish relevant states—in this case pre-lasso, pre-tadpole, and unfolded conformations. This is typically done by identifying a set of distinguishing

features or combined features, called collective variables. Although the pre-tadpole was not distinguished as a distinct state in the previous work,[25] we first tested the proposed Glu8 Ψ-dihedral angle combined with the Λ to see if they might differentiate pre-lasso structures (**Figure S5**). The probability distributions show that separating and classifying pre-lasso and pre-tadpole is not possible with these parameters. There is significant overlap in both the Λ values, which are small indicating the presence of the β-hairpin for all pre-lassos and many pre-tadpole structures, and Glu8 Ψ, which shows both conformations cluster around -40° and 150° (**Figure S5**). Thus, new descriptors were needed to distinguish pre-tadpole from pre-lasso conformations.

In order to clearly identify pre-lasso and pre-tadpole structures, we developed the lasso threading classification algorithm (**Figure 2**) combined with the criterion that the distance between the Gly1N and Glu8Cδ be less than 6 Å. While this algorithm unequivocally filters structures into one category or the other, it is not a differentiable variable essential for enhanced free energy sampling, or even a non-differentiable variable useful for plotting the phase space distribution. Instead, we tested the summation of ring-tail distances, using the alpha carbons of residues 1, 3, 6, and 8 to that of residue 19, combined with the Gly1N-Glu8Cδ distance to characterize conformational phase space (**Figure 6**).

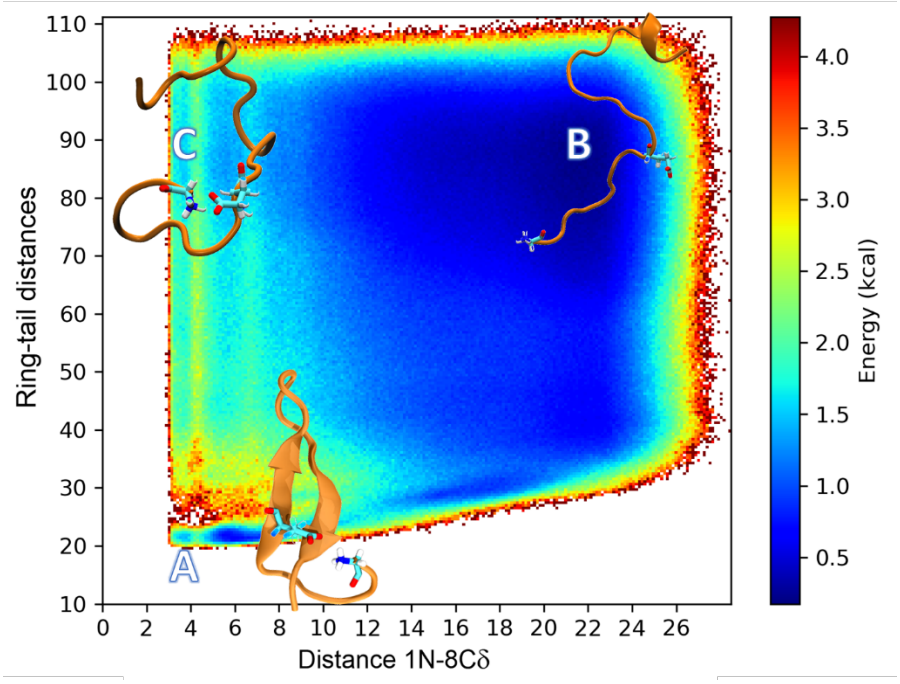

Figure 6: 2D free energy profile showing the distinct states pre-lasso (basin A), unfolded (basin B), and pre-tadpole (basin C) ensembles. The secondary structure of the peptide is represented in orange. The Gly1 and Glu8 residues are colored with carbons (teal), hydrogens (white), oxygens (red), and nitrogen (blue) for clarity.

The resulting 2D folding free energy landscape of all replicas ($-RT \ln \rho$, where ρ is the relative probability) demonstrates that the summation of distances between macrocyclic residues and the penetrating tail residue can distinguish the pre-lasso (basin A), unfolded (basin B), and pre-tadpole (basin C) ensembles. Focusing on only the filtered structures, where Gly1N-Glu8Cδ ≤ 6 Å, all replicas (**Figure S6-A**) show reasonable separation between the pre-lasso and pre-tadpole structures, with some degree of overlap as the ring-tail distance starts to increase. The overlapping pre-tadpoles share some conformational similarities with the pre-

lassos, like the β-hairpin preserved ($\Lambda < 7$) and less consistently a hydrogen bond between the backbone of the residues Val6-Tyr20. The ring-tail distance also presents a better separation than Glu8-Ψ when combined with Λ (**Figure S6-B**), highlighting the 6-20 hydrogen bond occurs with longer 1-8 distances but a tightly formed β-hairpin. While this combination of variables provides useful discretization of phase space, the overlap in pre-lasso and pre-tadpole distributions indicates these are not yet effective parameters for enhanced sampling simulations aiming to distinguish the probability of forming a lasso versus tadpole structure once the isopeptide bond forms. The identification of such parameters will be a valuable advance for future research. Collectively, the folding landscape (**Figure 6**) captures how the formation of the pre-lasso precursor is entropically disfavored. Both the broad unfolded phase space and pre-tadpole distributions dominate over the pre-lasso ensemble, which occupies a much narrower range within these parameters, reflective of the compact structure of the interlocked lasso motif.

Chemical modifications

One way to influence the stability of peptide conformations is by replacing native residues with unnatural modifications, which can also be used to permit chemoselective cyclization.[51-55] To examine the effect of modifications on pre-lasso peptide stability, we repeated the simulations from modified isopeptide bond-forming residues with an auxiliary attached to Gly1N (**Figure 7A**) and thioester functionalities at Glu8Cδ (**Figure 7BC**).

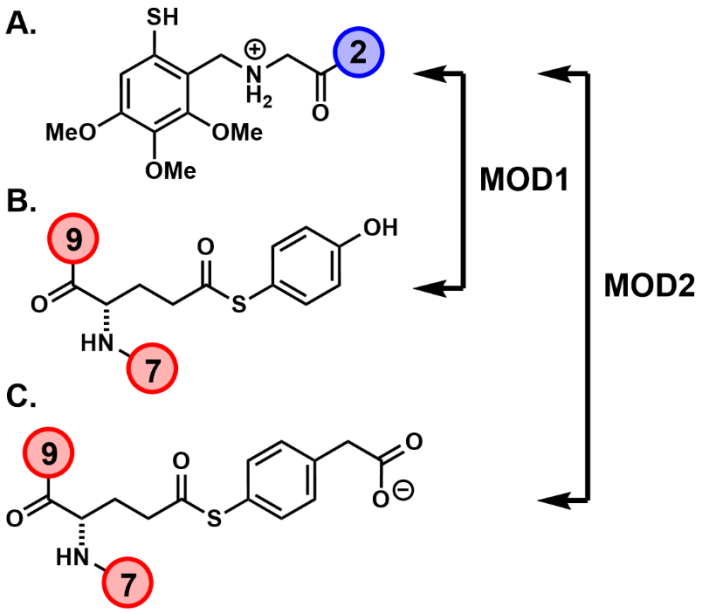

Figure 7: **A.** An auxiliary attached to Gly1N (blue) and **B./C.** thioester functionalities at Glu8Cδ (red). The two combinations are called **A, B.** MOD1 and **A, C.** MOD2.

In both cases, due to the introduction of auxiliary and thioester functionalities, an enlargement of the pre-lasso ring was necessary to mitigate steric hindrance during the minimization and equilibration process. The simulations were started with the peptide in pre-lasso conformation and run for similar times to the native peptide (**Table S2**). The resulting 2D free energy maps show marked differences for both the pre-lasso and pre-tadpole conformations (**Figure 8**). For MOD1, the proportion of pre-lasso and pre-tadpole configurations sampled from the entire trajectory increased from 4.1% to 13.5% (**Table S2**). Focusing on structures in pre-lasso and pre-tadpole ensembles, the percentage of pre-lassos

goes from 14.6% in the native state to 25.4% for MOD1. In the case of MOD2, there is a general increase from 4.1% to 6.7% in structures with Gly1 and Glu8 close together (**Table S2**). However, unlike the MOD1 combination, there is no increase in the proportion of lassoed conformations (14.6% vs. 3.7%). This combination of auxiliary and thioester promotes the most pronounced increase in the pre-tadpole set (3.5% to 6.5%).

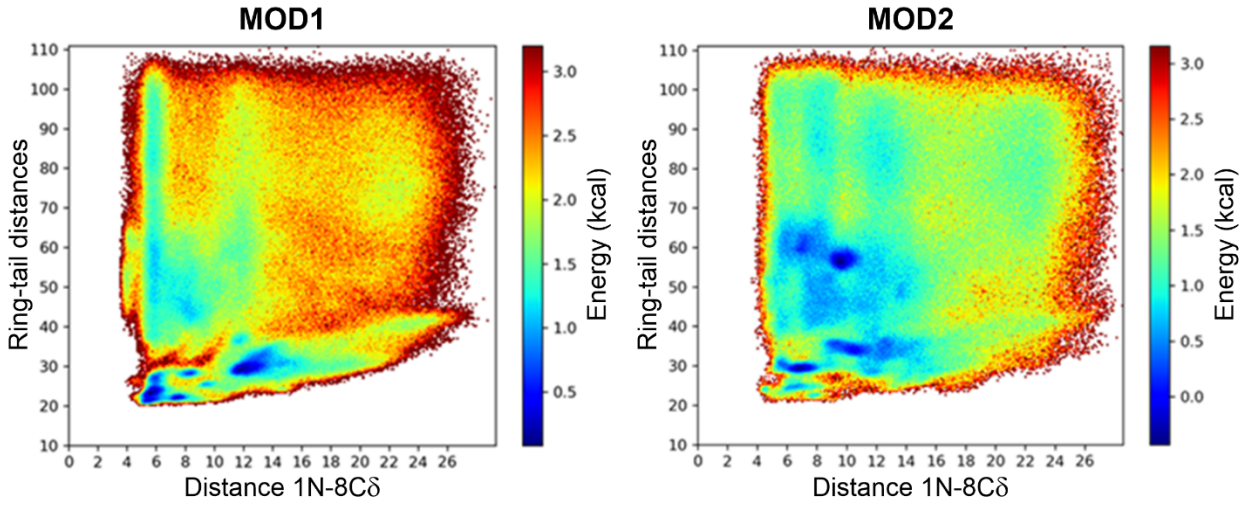

Figure 8: 2D histogram showing similar basins compared to the native state, but the pre-lasso region (basin A) is now larger for MOD1 and smaller for MOD2.

To understand the reason for increased pre-cyclic structures observed for MOD1, a cluster analysis was performed again with the DBSCAN algorithm and identified the most probable conformations in pre-lasso (**Figures 9-A and S7-A**) and pre-tadpole (**Figures 9-B and S7-B**) regions.

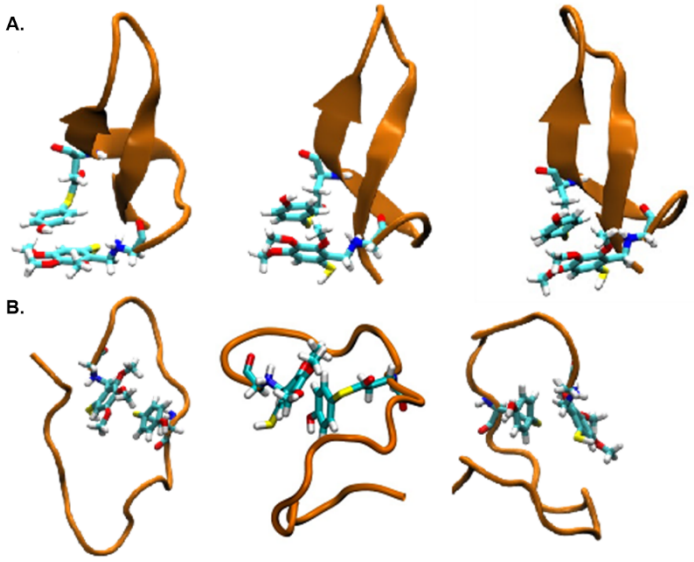

Figure 9: The three most populated clusters for **A.** pre-lassos (Pop0, Pop7, and Pop3) and **B.** pre-tadpoles (Pop0, Pop2, and Pop1), indicating the presence of π-π stacking in all structures. Other clusters observed were similar to those shown.

The dominant clusters involve π-π stacking of the substituents, suggesting such interactions promote pre-lasso stabilization. Contrary to the concern that larger substituents might introduce steric clashes and disfavor pre-ring assemblies, the π-π stacking of the MOD1 substituents seems to optimally match hydrophobic ring faces and solvated polar groups to reduce the likelihood of spontaneous pre-ring dissociation. This hypothesis is supported by the longer duration needed for the pre-lasso peptide to lose the β-hairpin and transition to unfolded structures, as indicated by the secondary structure pattern (**Figure S8**). In the pre-

lasso ensemble, additional clusters display sulfur interactions (**Figure S9**). Thus, the pre-lasso folding propensity can be significantly promoted by π-π stacking of the MOD1 moieties that is further augmented by sulfur interactions in the pre-lasso ensemble.

Despite the presence of π-π stacking interactions in the MOD2 pre-lasso clusters, the larger size of the MOD2 thioester side chain causes its carboxylate group to be closer to the backbone oxygen of the Gly1 auxiliary (**Figure S10**) than its $R_2NH_2^+$ group. This spatial arrangement creates a small but sufficient repulsion that decreases the stability of the pre-lasso ring relative to MOD1. With greater instability, the pre-ring opens, and the β-hairpin dissociates more readily. Once opened, the interactions of Gly1 and Glu8 residues via π-π stacking (**Figure S10**) stand out. The peptide then assumes several pre-tadpole forms, which are more numerous than those observed with the native sequence. Thus, modification of MccJ25 with auxiliary and thioester to Gly1 and Glu8 decreases the pre-lasso stability for MOD2, while MOD1 shows increased stabilization of the pre-lasso fold.

Influence of pH

In order to test the potential influence of side chain ionization on folding, we repeated our simulations starting from the native NMR solution structure, which exhibits a salt bridge with a protonated His5 residue and the *C*-terminus Gly21 carboxylate.[26] The imidazolium-bearing His5 could therefore attract the Gly21 carboxylate, contributing to the pre-lasso stability and might increase the hydrophilicity and solvation of the pre-ring. A 7.2 μs simulation resulted in a new free energy distribution for the protonated native sequence (**Figure 10**). Within the

filtered ensemble, structures with Gly1N and Glu8Cδ distances ≤ 6 Å, the protonation of His5 decreases the relative probability of pre-lasso to pre-tadpole structures from 14.6% to only 0.8% (**Table S2**). Despite this, the pre-tadpole population in the total trajectory is similar for neutral and protonated His5 (3.5% compared to 3.7%, respectively). Cumulatively, the protonation of His5 destabilizes the pre-lasso fold for native MccJ25 through increased solvation of the ring residues, which inhibits His5 Gly21 ring-tail interactions (further discussed below).

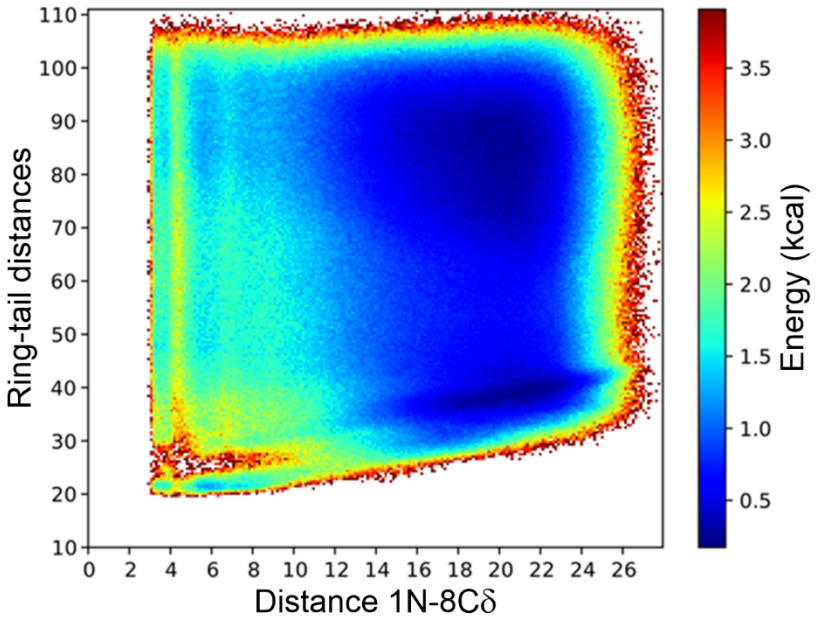

Figure 10: 2D free energy profile for the MccJ25 with protonated His5, analogous to that for neutral His5 in Figure 6.

Similarly, simulations starting from the pre-lasso with protonated His5 were run for MOD1 and MOD2 (**Figure S11**). There was a general increase in the total number of filtered structures from the entire trajectory in both cases going from 3.7% (WT) to 10.7% (MOD1) and 9.9% (MOD2) with His5 protonated (**Table S2**). From this set of structures, the percentage of pre-lassos in MOD1 significantly increases from 0.8% in the protonated native state to 45.6% (compared to 25.4% with neutral His5). On the other hand, MOD2 protonation decreased further from 3.7% (neutral His5) to 3.1% and promoted a pronounced increase of pre-tadpoles (6.5% of the total trajectory for neutral MOD2 to 9.6% with protonated MOD2).

Finally, we further evaluated the role of His5 on pre-lasso stability. Contact analysis of His5 with the ring residues 1-8 and tail residues 19-21, using a 4 Å cutoff to define a contact, shows consistent interactions with neighboring Val6 and Pro7 residues (**Figure S12**). However, native pre-MccJ25 shows fewer interactions with the tail residues when His5 is protonated compared to neutral. This result suggests that conditions favoring protonation and added hydrophilicity could increase the hydration of His5 and decrease its interactions with neighboring and tail residues.

This behavior changes, however, in simulations with MOD1, wherein protonated His5 interacts more with the tail residues. In particular, the last residue (Gly21) goes from 2-3 interactions in the neutral version to more than 20 interactions in the protonated peptide. The more hydrophilic character of His+ also influences this result as the side chain flipping out toward water molecules exposes the amide backbone such that it can hydrogen bond with the terminal carboxylate of Gly21. This interaction is facilitated by the enlargement in the ring

circumference due to the size of the auxiliary and the thioester groups on residues 1 and 8, which decreases the steric hindrance caused by Tyr20 and promotes folding of the loop/tail. Thus, His5+ interactions stabilize the pre-lasso through backbone hydrogen bonding to the terminal carboxylate and side chain hydration (**Figure 11**), suggesting that reaction conditions such as pH can facilitate stable pre-lasso folding.

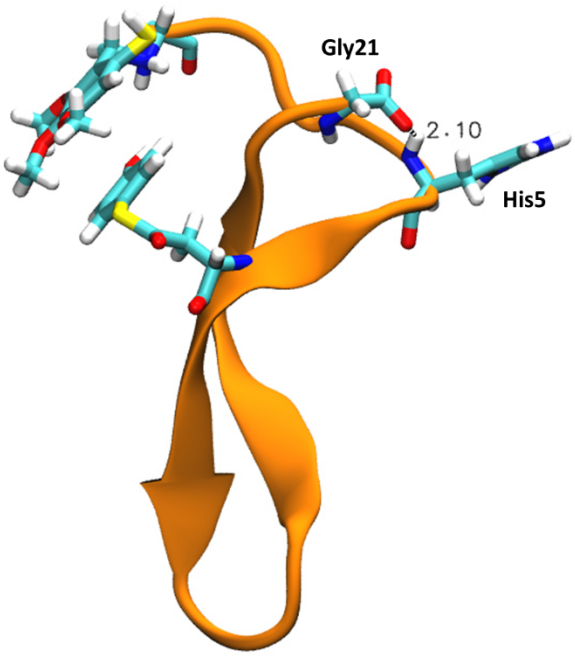

Figure 11: Snapshot of MccJ25 MOD1 His+ showing the Gly21 carboxyl group interacting with the backbone of His5+ with a hydrogen bond of 2.10 Å.

Collectively, alteration of the native residues in MccJ25 with unnatural modifications and ionizable groups significantly modulates the pre-lasso folding propensity. These findings

suggest that the rational design of lasso peptides can target variations in sequence, unnatural modifications, and ionizable functionalities to increase the stability of the pre-lasso fold.

CONCLUSIONS

Lasso peptides are compact structures with unique properties that have the potential to become scaffolds for therapeutic development. MccJ25 is a model lasso peptide due to its antimicrobial properties and unique β-hairpin within its folded structure. In nature, MccJ25, like all characterized natural lasso peptides, access their threaded structures enzymatically. However, the abiotic folding of lasso peptides *de novo* is underexplored. This work uses extensive MD simulations to revisit the folding propensity of MccJ25, which was previously suggested to rapidly transition to the unnatural left-handed structure. We find that improved force fields support the preference for the natural right-handed conformation and demonstrate increased access to the pre-lasso ensemble. For MccJ25, the observed preference for a right-handed pre-lasso may be the consequence of some, or all of the L-configured residues, that predispose the peptide to favor the right-handed structure. This right-handed predisposition, consistent with other natural lasso peptides, may be reinforced upon binding and cyclization as mediated by the lasso cyclase enzyme. Additional studies examining the effect of D-configured residue substitutions on pre-lasso handedness preference are needed. We present new tools employing triangulation and the barycentric transformation to definitively characterize pre-lasso conformations and distinguish handedness. These tools for

characterizing pre-lasso conformations could be used together with computational tools like LassoHTP, which predicts bonded lasso peptide structures and ensembles,[56] in future design strategies for lasso peptide diversification. We also demonstrate that chemical modification the ring-forming residues increases pre-lasso stabilization through π-π stacking and sulfur interactions. Similarly, His5 protonation further increases the pre-lasso ensemble stability. In this case, the increased hydrophilicity of imidazolium-bearing His5 reorients the backbone, enabling hydrogen bonding with the *C*-terminal Gly1 carboxylate. Importantly, our findings demonstrate that alteration of the sequence, incorporating unnatural modifications and ionizable functionalities could permit a rational design of lasso peptides. These developments mark the first steps toward realizing a generalizable platform for the chemical synthesis of lassos peptides, which could permit access to mirror-image lassos (from D-amino acids), and the incorporation of non-canonical residues, including D-amino acids, β-amino acids, peptoids, and others, to compliment biosynthetic approaches[19] that diversify these remarkable scaffolds toward the design of novel therapeutics.

ASSOCIATED CONTENT

Supporting Information.

The Supporting Information is available free of charge at https://pubs.acs.org/doi/10.1021/jacs.X

Simulation methods; algorithm descriptions and equations; parametrization protocol; cluster analyses; secondary structure analyses; Glu8 Ψ dihedral angle distributions; number of pre-lasso and pre-tadpole structures across different force fields; contact map analyses; 2-D probability distributions for multiple replicas; distribution of filtered structures based on the distance 1N-8Cδ vs. LAMBDA; total number of structures for each simulation and the ratio between pre-lassos and pre-tadpoles; cluster and secondary structure analyses for MOD1; 2-D energy maps for the MOD1 and MOD2 with His5+; contact analyses for His5; Tables S1-S2; and Figures S1-S12 (PDF).

AUTHOR INFORMATION

Corresponding Author

* **Jessica M. J. Swanson** - Department of Chemistry, University of Utah, Salt Lake City, UT, 84112 – United States, Email: j.swanson@utah.edu; https://orcid.org/0000-0002-9820-1307

Authors

Gabriel C. A. da Hora - Department of Chemistry, University of Utah, Salt Lake City, UT, 84112 – United States; https://orcid.org/0000-0002-6372-6533

Myongin Oh - Department of Chemistry, University of Utah, Salt Lake City, UT, 84112 – United States; https://orcid.org/0000-0003-1145-5142

Marcus C. Mifflin - Department of Chemistry, University of Utah, Salt Lake City, UT, 84112 – United States; https://orcid.org/0000-0002-5283-9663

Lori Digal - Department of Chemistry, University of Utah, Salt Lake City, UT, 84112 – United States

Andrew G. Roberts - Department of Chemistry, University of Utah, Salt Lake City, UT, 84112 – United States; https://orcid.org/0000-0002-2221-534X

Present Addresses

† **Myongin Oh** - Weill Cornell Medicine, 1300 York Ave, New York, NY 10065, United States;

Notes

The authors declare no competing financial interest.

ACKNOWLEDGMENT

The authors thank Prof. Dr. Anselm Horn for the parameter set for the isopeptide bond between the Gly1 and Glu8. The authors would like to acknowledge the support from NIH NIGMS (R35GM143117) and the computational resources provided by Bridges-2 at the Pittsburgh Supercomputing Center through the ACCESS program (allocation MCB200018) supported by NSF (grants #2138259, #2138286, #2138307, #2137603, and #2138296), as well as

the Center for High Performance Computing (CHPC) at the University of Utah. These resources greatly aided in the completion of this research.

REFERENCES

(1) Arnison, P. G.; Bibb, M. J.; Bierbaum, G.; Bowers, A. A.; Bugni, T. S.; Bulaj, G.; Camarero, J. A.; Campopiano, D. J.; Challis, G. L.; Clardy, J.; et al. Ribosomally synthesized and post-translationally modified peptide natural products: overview and recommendations for a universal nomenclature. *Natural Product Reports* **2013**, *30* (1), 108-160, 10.1039/C2NP20085F. DOI: 10.1039/C2NP20085F.

(2) Hegemann, J. D.; Zimmermann, M.; Xie, X.; Marahiel, M. A. Lasso Peptides: An Intriguing Class of Bacterial Natural Products. *Accounts of Chemical Research* **2015**, *48* (7), 1909-1919. DOI: 10.1021/acs.accounts.5b00156 From NLM Medline.

(3) Kretsch, A. M.; Gadgil, M. G.; DiCaprio, A. J.; Barrett, S. E.; Kille, B. L.; Si, Y.; Zhu, L.; Mitchell, D. A. Peptidase Activation by a Leader Peptide-Bound RiPP Recognition Element. *Biochemistry* **2023**, *62* (4), 956-967. DOI: 10.1021/acs.biochem.2c00700 From NLM Medline.

(4) Ongpipattanakul, C.; Desormeaux, E. K.; DiCaprio, A.; van der Donk, W. A.; Mitchell, D. A.; Nair, S. K. Mechanism of Action of Ribosomally Synthesized and Post-Translationally Modified Peptides. *Chemical Reviews* **2022**, *122* (18), 14722-14814. DOI: 10.1021/acs.chemrev.2c00210 From NLM Medline.

(5) Cortés-Albayay, C.; Jarmusch, S. A.; Trusch, F.; Ebel, R.; Andrews, B. A.; Jaspars, M.; Asenjo, J. A. Downsizing Class II Lasso Peptides: Genome Mining-Guided Isolation of Huascopeptin Containing the First Gly1-Asp7 Macrocycle. *The Journal of Organic Chemistry* **2020**, *85* (3), 1661-1667. DOI: 10.1021/acs.joc.9b02231 From NLM Medline.

(6) Cheung-Lee, W. L.; Cao, L.; Link, A. J. Pandonodin: A Proteobacterial Lasso Peptide with an Exceptionally Long C-Terminal Tail. *ACS Chemical Biology* **2019**, *14* (12), 2783-2792. DOI: 10.1021/acschembio.9b00676 From NLM Medline.

(7) Si, Y.; Kretsch, A. M.; Daigh, L. M.; Burk, M. J.; Mitchell, D. A. Cell-Free Biosynthesis to Evaluate Lasso Peptide Formation and Enzyme–Substrate Tolerance. *Journal of the American Chemical Society* **2021**, *143* (15), 5917-5927. DOI: 10.1021/jacs.1c01452.

(8) Tietz, J. I.; Schwalen, C. J.; Patel, P. S.; Maxson, T.; Blair, P. M.; Tai, H.-C.; Zakai, U. I.; Mitchell, D. A. A new genome-mining tool redefines the lasso peptide biosynthetic landscape. *Nature Chemical Biology* **2017**, *13* (5), 470-478. DOI: 10.1038/nchembio.2319 From NLM Medline.

(9) Burkhart, B. J.; Hudson, G. A.; Dunbar, K. L.; Mitchell, D. A. A prevalent peptide-binding domain guides ribosomal natural product biosynthesis. *Nature Chemical Biology* **2015**, *11* (8), 564-570. DOI: 10.1038/nchembio.1856.

(10) Yan, K. P.; Li, Y.; Zirah, S.; Goulard, C.; Knappe, T. A.; Marahiel, M. A.; Rebuffat, S. Dissecting the maturation steps of the lasso peptide microcin J25 in vitro. *Chembiochem* **2012**, *13* (7), 1046-1052. DOI: 10.1002/cbic.201200016 From NLM Medline.

(11) Potterat, O.; Wagner, K.; Gemmecker, G.; Mack, J.; Puder, C.; Vettermann, R.; Streicher, R. BI-32169, a Bicyclic 19-Peptide with Strong Glucagon Receptor Antagonist Activity from Streptomyces sp. *Journal of Natural Products* **2004**, *67* (9), 1528-1531. DOI: 10.1021/np040093o.

(12) Salomón, R. A.; Farías, R. N. Microcin 25, a novel antimicrobial peptide produced by Escherichia coli. *J Bacteriol* **1992**, *174* (22), 7428-7435. DOI: 10.1128/jb.174.22.7428-7435.1992 From NLM.

(13) Kodani, S.; Unno, K. How to harness biosynthetic gene clusters of lasso peptides. *Journal of Industrial Microbiology and Biotechnology* **2020**, *47* (9-10), 703-714. DOI: 10.1007/s10295-020-02292-6 (acccessed 9/1/2023). From NLM Medline.

(14) Kimura, K.; Kanou, F.; Takahashi, H.; Esumi, Y.; Uramoto, M.; Yoshihama, M. Propeptin, a new inhibitor of prolyl endopeptidase produced by Microbispora. I. Fermentation, isolation and biological properties. *J. Antibiot.* **1997**, *50* (5), 373-378. DOI: 10.7164/antibiotics.50.373 (acccessed 2023/09/01/02:00:02). From NLM Medline.

(15) Martin-Gómez, H.; Tulla-Puche, J. Lasso peptides: chemical approaches and structural elucidation. *Organic & Biomolecular Chemistry* **2018**, *16* (28), 5065-5080, 10.1039/C8OB01304G. DOI: 10.1039/C8OB01304G From NLM PubMed-not-MEDLINE.

(16) Liu, T.; Ma, X.; Yu, J.; Yang, W.; Wang, G.; Wang, Z.; Ge, Y.; Song, J.; Han, H.; Zhang, W.; et al. Rational generation of lasso peptides based on biosynthetic gene mutations and site-selective chemical modifications. *Chemical Science* **2021**, *12* (37), 12353-12364, 10.1039/D1SC02695J. DOI: 10.1039/D1SC02695J From NLM PubMed-not-MEDLINE.

(17) Vinogradov, A. A.; Yin, Y.; Suga, H. Macrocyclic Peptides as Drug Candidates: Recent Progress and Remaining Challenges. *J Am Chem Soc* **2019**, *141* (10), 4167-4181. DOI: 10.1021/jacs.8b13178 From NLM Medline.

(18) Zong, C.; Maksimov, M. O.; Link, A. J. Construction of Lasso Peptide Fusion Proteins. *ACS Chemical Biology* **2016**, *11* (1), 61-68. DOI: 10.1021/acschembio.5b00745 From NLM Medline.

(19) Knappe, T. A.; Manzenrieder, F.; Mas-Moruno, C.; Linne, U.; Sasse, F.; Kessler, H.; Xie, X.; Marahiel, M. A. Introducing lasso peptides as molecular scaffolds for drug design: engineering of an integrin antagonist. *Angew Chem Int Ed Engl* **2011**, *50* (37), 8714-8717. DOI: 10.1002/anie.201102190 From NLM Medline.

(20) Hegemann, J. D. Factors Governing the Thermal Stability of Lasso Peptides. *Chembiochem* **2020**, *21* (1-2), 7-18. DOI: 10.1002/cbic.201900364 From NLM Medline.

(21) Mevaere, J.; Goulard, C.; Schneider, O.; Sekurova, O. N.; Ma, H.; Zirah, S.; Afonso, C.; Rebuffat, S.; Zotchev, S. B.; Li, Y. An orthogonal system for heterologous expression of actinobacterial lasso peptides in Streptomyces hosts. *Scientific Reports* **2018**, *8* (1), 8232. DOI: 10.1038/s41598-018-26620-0 From NLM Medline.

(22) DiCaprio, A. J.; Firouzbakht, A.; Hudson, G. A.; Mitchell, D. A. Enzymatic Reconstitution and Biosynthetic Investigation of the Lasso Peptide Fusilassin. *Journal of the American Chemical Society* **2019**, *141* (1), 290-297. DOI: 10.1021/jacs.8b09928 From NLM Medline.

(23) Al Toma, R. S.; Kuthning, A.; Exner, M. P.; Denisiuk, A.; Ziegler, J.; Budisa, N.; Sussmuth, R. D. Site-directed and global incorporation of orthogonal and isostructural noncanonical amino acids into the ribosomal lasso peptide capistruin. *Chembiochem* **2015**, *16* (3), 503-509. DOI: 10.1002/cbic.201402558 From NLM Medline.

(24) Pan, S. J.; Link, A. J. Sequence Diversity in the Lasso Peptide Framework: Discovery of Functional Microcin J25 Variants with Multiple Amino Acid Substitutions. *Journal of the American Chemical Society* **2011**, *133* (13), 5016-5023. DOI: 10.1021/ja1109634 From NLM Medline.

(25) Ferguson, A. L.; Zhang, S.; Dikiy, I.; Panagiotopoulos, A. Z.; Debenedetti, P. G.; Link, A. J. An experimental and computational investigation of spontaneous lasso formation in microcin J25. *Biophysical Journal* **2010**, *99* (9), 3056-3065. DOI: 10.1016/j.bpj.2010.08.073.

(26) Rosengren, K. J.; Clark, R. J.; Daly, N. L.; Göransson, U.; Jones, A.; Craik, D. J. Microcin J25 Has a Threaded Sidechain-to-Backbone Ring Structure and Not a Head-to-Tail Cyclized Backbone. *Journal of the American Chemical Society* **2003**, *125* (41), 12464-12474. DOI: 10.1021/ja0367703.

(27) Lear, S.; Munshi, T.; Hudson, A. S.; Hatton, C.; Clardy, J.; Mosely, J. A.; Bull, T. J.; Sit, C. S.; Cobb, S. L. Total chemical synthesis of lassomycin and lassomycin-amide. *Organic & Biomolecular Chemistry* **2016**, *14* (19), 4534-4541, 10.1039/C6OB00631K. DOI: 10.1039/C6OB00631K From NLM Medline.

(28) Waliczek, M.; Wierzbicka, M.; Arkuszewski, M.; Kijewska, M.; Jaremko, Ł.; Rajagopal, P.; Szczepski, K.; Sroczyńska, A.; Jaremko, M.; Stefanowicz, P. Attempting to synthesize lasso peptides using high pressure. *PLOS ONE* **2020**, *15* (6), e0234901. DOI: 10.1371/journal.pone.0234901 From NLM Medline.

(29) Soudy, R.; Wang, L.; Kaur, K. Synthetic peptides derived from the sequence of a lasso peptide microcin J25 show antibacterial activity. *Bioorg Med Chem* **2012**, *20* (5), 1794-1800. DOI: 10.1016/j.bmc.2011.12.061 From NLM Medline.

(30) Braffman, N. R.; Piscotta, F. J.; Hauver, J.; Campbell, E. A.; Link, A. J.; Darst, S. A. Structural mechanism of transcription inhibition by lasso peptides microcin J25 and capistruin. *Proceedings of the National Academy of Sciences* **2019**, *116* (4), 1273-1278. DOI: doi:10.1073/pnas.1817352116.

(31) Piscotta, F. J.; Tharp, J. M.; Liu, W. R.; Link, A. J. Expanding the chemical diversity of lasso peptide MccJ25 with genetically encoded noncanonical amino acids. *Chemical Communications* **2015**, *51* (2), 409-412, 10.1039/C4CC07778D. DOI: 10.1039/C4CC07778D.

(32) Lai, P.-K.; Kaznessis, Y. N. Free Energy Calculations of Microcin J25 Variants Binding to the FhuA Receptor. *Journal of Chemical Theory and Computation* **2017**, *13* (7), 3413-3423. DOI: 10.1021/acs.jctc.7b00417.

(33) de Cristóbal, R. E.; Solbiati, J. O.; Zenoff, A. M.; Vincent, P. A.; Salomón, R. A.; Yuzenkova, J.; Severinov, K.; Farías, R. N. Microcin J25 uptake: His5 of the MccJ25 lariat ring is involved in interaction with the inner membrane MccJ25 transporter protein SbmA. *J Bacteriol* **2006**, *188* (9), 3324-3328. DOI: 10.1128/jb.188.9.3324-3328.2006 From NLM.

(34) Bellomio, A.; Vincent, P. A.; de Arcuri, B. F.; Farías, R. N.; Morero, R. D. Microcin J25 has dual and independent mechanisms of action in Escherichia coli: RNA polymerase inhibition and increased superoxide production. *J Bacteriol* **2007**, *189* (11), 4180-4186. DOI: 10.1128/jb.00206-07 From NLM.

(35) Pavlova, O.; Mukhopadhyay, J.; Sineva, E.; Ebright, R. H.; Severinov, K. Systematic structure-activity analysis of microcin J25. *J Biol Chem* **2008**, *283* (37), 25589-25595. DOI: 10.1074/jbc.M803995200 PubMed.

(36) Dabrowski-Tumanski, P.; Niemyska, W.; Pasznik, P.; Sulkowska, J. I. LassoProt: server to analyze biopolymers with lassos. *Nucleic Acids Research* **2016**, *44* (W1), W383-W389. DOI: 10.1093/nar/gkw308 (acccessed 9/9/2023). From NLM Medline.

(37) Soares, T. A.; Daura, X.; Oostenbrink, C.; Smith, L. J.; van Gunsteren, W. F. Validation of the GROMOS force-field parameter set 45A3 against nuclear magnetic resonance data of hen egg lysozyme. *Journal of Biomolecular NMR* **2004**, *30* (4), 407-422. DOI: 10.1007/s10858-004-5430-1 From NLM Medline.

(38) Schmid, N.; Eichenberger, A. P.; Choutko, A.; Riniker, S.; Winger, M.; Mark, A. E.; van Gunsteren, W. F. Definition and testing of the GROMOS force-field versions 54A7 and 54B7. *Eur Biophys J* **2011**, *40* (7), 843-856. DOI: 10.1007/s00249-011-0700-9 From NLM Medline.

(39) Oostenbrink, C.; Soares, T. A.; van der Vegt, N. F. A.; van Gunsteren, W. F. Validation of the 53A6 GROMOS force field. *European Biophysics Journal : EBJ* **2005**, *34* (4), 273-284. DOI: 10.1007/s00249-004-0448-6.

(40) Schuler, L. D.; Daura, X.; van Gunsteren, W. F. An improved GROMOS96 force field for aliphatic hydrocarbons in the condensed phase. *Journal of Computational Chemistry* **2001**, *22* (11), 1205-1218. DOI: 10.1002/jcc.1078.

(41) Niemyska, W.; Dabrowski-Tumanski, P.; Kadlof, M.; Haglund, E.; Sulkowski, P.; Sulkowska, J. I. Complex lasso: New entangled motifs in proteins. *Scientific Reports* **2016**, *6* (1), 1-10. DOI: 10.1038/srep36895.

(42) Chen, W.; Cai, Y.; Zheng, J. Constructing triangular meshes of minimal area. *Computer-Aided Design and Applications* **2008**, *5* (1-4), 508-518. DOI: 10.3722/cadaps.2008.508-518.

(43) Ester, M.; Kriegel, H.-P.; Sander, J.; Xu, X. A density-based algorithm for discovering clusters in large spatial databases with noise. In Proceedings of the Second International Conference on Knowledge Discovery and Data Mining, Portland, Oregon; 1996.

(44) Ferguson, A. L.; Panagiotopoulos, A. Z.; Debenedetti, P. G.; Kevrekidis, I. G. Systematic determination of order parameters for chain dynamics using diffusion maps. *Proceedings of the National Academy of Sciences* **2010**, *107* (31), 13597-13602. DOI: doi:10.1073/pnas.1003293107 From NLM Medline.

(45) Yang, S.; Onuchic, J. N.; García, A. E.; Levine, H. Folding time predictions from all-atom replica exchange simulations. *J Mol Biol* **2007**, *372* (3), 756-763. DOI: 10.1016/j.jmb.2007.07.010 From NLM Medline.

(46) Maier, J. A.; Martinez, C.; Kasavajhala, K.; Wickstrom, L.; Hauser, K. E.; Simmerling, C. ff14SB: Improving the Accuracy of Protein Side Chain and Backbone Parameters from ff99SB. *Journal of Chemical Theory and Computation* **2015**, *11* (8), 3696-3713. DOI: 10.1021/acs.jctc.5b00255.

(47) Huang, J.; Mackerell, A. D. CHARMM36 all-atom additive protein force field: Validation based on comparison to NMR data. *Journal of Computational Chemistry* **2013**, *34* (25), 2135-2145. DOI: 10.1002/jcc.23354.

(48) Huang, J.; Rauscher, S.; Nawrocki, G.; Ran, T.; Feig, M.; De Groot, B. L.; Grubmüller, H.; MacKerell, A. D. CHARMM36m: An improved force field for folded and intrinsically disordered proteins. *Nature Methods* **2016**, *14* (1), 71-73. DOI: 10.1038/nmeth.4067.

(49) Abraham, M. J.; Murtola, T.; Schulz, R.; Páll, S.; Smith, J. C.; Hess, B.; Lindah, E. Gromacs: High performance molecular simulations through multi-level parallelism from laptops to supercomputers. *SoftwareX* **2015**, *1-2*, 19-25. DOI: 10.1016/j.softx.2015.06.001.

(50) Schuler, L. D.; Van Gunsteren, W. F. On the Choice of Dihedral Angle Potential Energy Functions for n-Alkanes. *Molecular Simulation* **2000**, *25* (5), 301-319. DOI: 10.1080/08927020008024504.

(51) Agouridas, V.; El Mahdi, O.; Diemer, V.; Cargoët, M.; Monbaliu, J.-C. M.; Melnyk, O. Native Chemical Ligation and Extended Methods: Mechanisms, Catalysis, Scope, and Limitations. *Chemical Reviews* **2019**, *119* (12), 7328-7443. DOI: 10.1021/acs.chemrev.8b00712 From NLM PubMed-not-MEDLINE.

(52) Merritt, H. I.; Sawyer, N.; Arora, P. S. Bent Into Shape: Folded Peptides to Mimic Protein Structure and Modulate Protein Function. *Pept Sci (Hoboken)* **2020**, *112* (1), e24145. DOI: 10.1002/pep2.24145 From NLM PubMed-not-MEDLINE.

(53) Barnes, N. G.; Nyandoro, K.; Jin, H.; Macmillan, D. Rapid access to Asp/Glu sidechain hydrazides as thioester precursors for peptide cyclization and glycosylation. *Chemical*

Communications **2021**, *57* (8), 1006-1009, 10.1039/D0CC07404G. DOI: 10.1039/D0CC07404G From NLM Medline.

(54) Johnson, E. C. B.; Kent, S. B. H. Insights into the Mechanism and Catalysis of the Native Chemical Ligation Reaction. *Journal of the American Chemical Society* **2006**, *128* (20), 6640-6646. DOI: 10.1021/ja058344i From NLM Medline.

(55) Offer, J.; Boddy, C. N. C.; Dawson, P. E. Extending Synthetic Access to Proteins with a Removable Acyl Transfer Auxiliary. *Journal of the American Chemical Society* **2002**, *124* (17), 4642-4646. DOI: 10.1021/ja016731w From NLM Medline.

(56) Juarez, R. J.; Jiang, Y.; Tremblay, M.; Shao, Q.; Link, A. J.; Yang, Z. J. LassoHTP: A High-Throughput Computational Tool for Lasso Peptide Structure Construction and Modeling. *J Chem Inf Model* **2023**, *63* (2), 522-530. DOI: 10.1021/acs.jcim.2c00945 From NLM Medline.